

Detection of molecular gas in an ALMA [C II]-identified submillimetre galaxy at $z = 4.44$

M. T. Huynh,^{1★} A. E. Kimball,² R. P. Norris,² Ian Smail,³ K. E. Chow,²
K. E. K. Coppin,⁴ B. H. C. Emonts,^{2,5} R. J. Ivison,^{6,7} V. Smolčić^{6,8,9}
and A. M. Swinbank³

¹ International Centre for Radio Astronomy Research, M468, University of Western Australia, Crawley, WA 6009, Australia

² CSIRO Astronomy and Space Science, PO Box 76, Epping, NSW 1710, Australia

³ Institute for Computational Cosmology, Department of Physics, Durham University, Durham DH1 3LE, UK

⁴ Centre for Astrophysics, University of Hertfordshire, College Lane, Hatfield, Hertfordshire AL10 9AB, UK

⁵ Centro de Astrobiología (INTA-CSIC), Ctra de Torrejón a Ajalvir, km 4, E-28850 Torrejón de Ardoz, Madrid, Spain

⁶ European Southern Observatory, Karl Schwarzschild Strasse 2, D-85748 Garching, Germany

⁷ Institute for Astronomy, University of Edinburgh, Royal Observatory, Blackford Hill, Edinburgh EH9 3HJ, UK

⁸ Argelander Institut für Astronomy, Auf dem Hugel 71, D-53121 Bonn, Germany

⁹ Physics Department, University of Zagreb, Bijenička cesta 32, 10002 Zagreb, Croatia

Accepted 2014 May 27. Received 2014 May 21; in original form 2014 April 22

ABSTRACT

We present the detection of $^{12}\text{CO}(2-1)$ in the $z = 4.44$ submillimetre galaxy ALESS65.1 using the Australia Telescope Compact Array. A previous Atacama Large Millimeter/submillimeter Array study of submillimetre galaxies (SMGs) in the Extended *Chandra* Deep Field South determined the redshift of this optically and near-infrared undetected source through the measurement of [C II] 157.74 μm emission. Using the luminosity of the $^{12}\text{CO}(2-1)$ emission, we estimate the gas mass to be $M_{\text{gas}} \sim 1.7 \times 10^{10} M_{\odot}$. The gas depletion time-scale of ALESS65.1 is ~ 25 Myr, similar to other high-redshift SMGs and consistent with $z > 4$ SMGs being the progenitors of massive ‘red-and-dead’ galaxies at $z > 2$. The ratio of the [C II], ^{12}CO and far-infrared luminosities implies a strong far-ultraviolet field of $G_0 \sim 10^{3.25}$, which is at the high end of the far-ultraviolet fields seen in local starbursts, but weaker than the far-ultraviolet fields of most nearby ultraluminous infrared galaxies (ULIRGs). The high ratio of $L_{[\text{C II}]} / L_{\text{FIR}} = 1.0 \times 10^{-3}$ observed in ALESS65.1, combined with $L_{[\text{C II}]} / L_{\text{CO}} \sim 2300$, is consistent with ALESS65.1 having more extended regions of intense star formation than local ULIRGs.

Key words: galaxies: evolution – galaxies: formation – radio lines: galaxies.

1 INTRODUCTION

Submillimetre galaxies (SMGs) are a population of ultraluminous infrared galaxies (ULIRGs) with extreme star formation rates (SFRs) of $100\text{--}1000 M_{\odot} \text{ yr}^{-1}$ (e.g. Blain et al. 2002) with typical redshifts of $z \sim 2.5$ (e.g. Chapman et al. 2005; Wardlow et al. 2011; Smolčić et al. 2012; Yun et al. 2012; Simpson et al. 2014). About 20 per cent of SMGs lie at $z > 4$ (Wardlow et al. 2011; Smolčić et al. 2012; Simpson et al. 2014), and a few dozen of these have now been studied in detail (Capak et al. 2008, 2011; Coppin et al. 2009; Daddi et al. 2009a,b; Carilli et al. 2010, 2011; Knudsen et al. 2010; Riechers et al. 2010; Cox et al. 2011; Smolčić et al. 2011; Combes et al. 2012; Walter et al. 2012; Vieira et al. 2013; Weiß et al. 2013). These sources are interesting as they represent the earliest examples of extreme starburst events in massive galaxies, and

knowledge of their star formation activity and gas content is crucial for understanding the growth of massive ellipticals.

Radio emission produced by the rotational transition of carbon monoxide (^{12}CO) is one of the most accessible tracers of cold molecular gas in galaxies (Carilli & Walter 2013). Detections of ^{12}CO in $z > 4$ SMGs have shown that they are gas-rich systems with sufficient reservoirs ($M_{\text{gas}} > 10^{10} M_{\odot}$) to sustain the extreme SFRs of $\sim 1000 M_{\odot} \text{ yr}^{-1}$ for only short time-scales (tens of Myr; Coppin et al. 2010; Riechers et al. 2010; Huynh et al. 2013), unless the gas is replenished. High-redshift SMGs are therefore seen as the likely progenitors of the luminous red galaxies seen at $z > 2$ (Cimatti et al. 2008).

A powerful emission line for studying the interstellar medium (ISM) of high-redshift sources is the $^2\text{P}_{3/2}\text{--}^2\text{P}_{1/2}$ fine-structure line of singly ionized carbon at 157.74 μm (hereafter [C II]), which can represent up to 1 per cent of the bolometric luminosity of star-forming galaxies (e.g. Crawford et al. 1985; Stacey et al. 1991). This line emission arises predominately from the edges of

* E-mail: minh.huynh@uwa.edu.au

molecular clouds illuminated by the UV photons of young massive stars (i.e. photodissociation regions), but a non-negligible contribution can also come from H II regions and the more diffuse warm ISM (Madden et al. 1993; Heiles 1994). The [C II] line therefore provides an important probe of the physical conditions in the ISM of a galaxy. This carbon line has now been studied in several high-redshift SMGs (De Breuck et al. 2011; Wagg et al. 2012; Walter et al. 2012; De Breuck et al. 2014; Rawle et al. 2014).

An Atacama Large Millimeter/submillimeter Array (ALMA) Cycle 0 study of 126 submillimetre sources located in the LABOCA Extended *Chandra* Deep Field South (LESS, Weiß et al. 2009; Hodge et al. 2013; Karim et al. 2013) resulted in the serendipitous identification of [C II] line emission from two SMGs (Swinbank et al. 2012, hereafter S12). The high [C II]/far-infrared (FIR) luminosity ratio of these two SMGs, roughly 10 times higher than that observed in local ULIRGs, was interpreted as evidence that their gas reservoirs are more extended (S12). High [C II]/FIR ratios (Ivison et al. 2010b; Stacey et al. 2010; S12) add to the mounting evidence that star formation in SMGs takes place in a region larger than the compact nuclear starbursts of local ULIRGs, which includes extended radio morphologies (e.g. Chapman et al. 2004; Biggs & Ivison 2008), extended H α morphologies (e.g. Swinbank et al. 2006), and large $^{12}\text{CO}(1-0)$ sizes (e.g. Ivison et al. 2010a; Hodge et al. 2012).

In Huynh et al. (2013), we presented Australia Telescope Compact Array (ATCA) observations, totalling about 20 h on-source, of one of the ALMA detected SMGs, ALESS J033252.26-273526.3 (hereafter ALESS65.1). No $^{12}\text{CO}(2-1)$ emission was detected but we were able to place constraints on the gas mass and physical conditions of the gas using the ALMA [C II] detection. Further observations were obtained with the ATCA in 2013 and, combined with the previous data, we now have detection of $^{12}\text{CO}(2-1)$. This Letter presents the ATCA observations, data analysis, and a discussion of the physical parameters derived from the molecular gas detection. We adopt the standard Λ cold dark matter cosmological parameters of $\Omega_M = 0.27$, $\Omega_\Lambda = 0.73$, and a Hubble constant of $71 \text{ km s}^{-1} \text{ Mpc}^{-1}$ throughout this Letter.

2 OBSERVATIONS AND RESULTS

The $^{12}\text{CO}(2-1)$ line ($\nu_{\text{rest}} = 230.538 \text{ GHz}$) in ALESS65.1 (RA = $03^{\text{h}}32^{\text{m}}52^{\text{s}}.26$, Dec. = $-27^{\circ}35'26''.3$, J2000; S12) was observed

over a period of four nights in 2012 August and three nights in 2013 July with the ATCA, using the Compact Array Broadband Backend (CABB). During both runs, the array was in the most compact five-antenna configuration, H75, which has a maximum baseline of 89 m and two antennas set along a northern spur. This hybrid configuration allows good (u, v) coverage to be obtained for integrations less than the full 12 h synthesis. The 7 mm receiver was centered on 42.343 GHz, the expected frequency of the $^{12}\text{CO}(2-1)$ line emission given the [C II] redshift of $z = 4.4445$ (S12). The 2 GHz bandwidth of CABB results in a frequency coverage of approximately 41.3–43.3 GHz, covering $^{12}\text{CO}(2-1)$ emission between $z = 4.32$ –4.58. The weather was average to good, with rms atmospheric path length variations of 100–400 μm throughout the runs, as measured on the 230 m baseline ATCA Seeing Monitor (Middelberg, Sault, & Kesteven 2006). Following Emonts et al. (2011), a bandpass calibration scan was acquired at the beginning and end of each 8 h night. Phase and amplitude calibration information was acquired with 2 min scans on PKS 0346–279 every 10 min and pointing checks performed on the same source every hour. For flux calibration, we observed Uranus at the beginning of the nights, at an elevation of ~ 55 deg. The uncertainty in the flux-density calibration using the standard MIRIAD model of Uranus is estimated to be 30 per cent (Emonts et al. 2011).

The data were calibrated, mapped and analysed using the standard MIRIAD (Sault & Killeen 1999) and KARMA (Gooch 1996) packages. The synthesized beam from natural weighting is $14.0 \times 9.0 \text{ arcsec}^2$. A total of about 40 h on-source integration time was obtained over the 7×8 h nights. ALESS65.1 was not detected in the 42.3 GHz continuum map from the full CABB band, which achieves an rms noise level of $7.4 \mu\text{Jy beam}^{-1}$.

The resultant channel noise in the 1 MHz (7.1 km s^{-1}) wide spectrum is $\sim 0.29 \text{ mJy beam}^{-1}$, consistent with other comparable 7 mm ATCA/CABB surveys (e.g. Coppin et al. 2010; Emonts et al. 2014) and the ATCA online sensitivity calculator. The visibilities were re-sampled to velocity resolutions of 200, 400 and 600 km s^{-1} and each cube was examined for an emission line near the ALMA position. The spectra at the source position in the 200, 400 and 600 km s^{-1} binned cubes (Fig. 1) have an rms of 0.057, 0.042 and 0.031 mJy beam^{-1} , respectively. We identify a line at the ALMA position and redshift in all three cubes. The line is detected at more than the 3σ level across multiple channels in the 200 and 400 km s^{-1} cubes

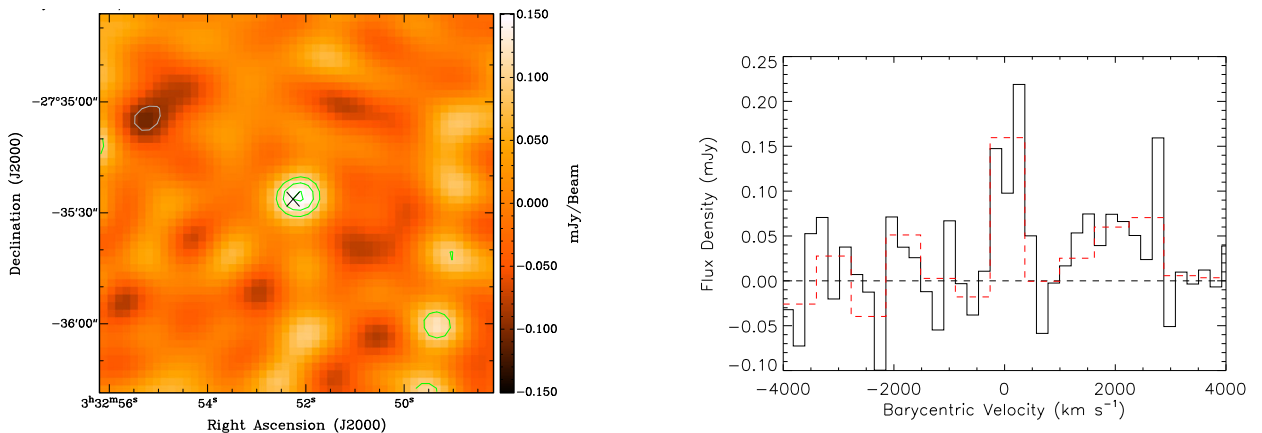


Figure 1. Left: $^{12}\text{CO}(2-1)$ emission line map of ALESS65.1, using 600 km s^{-1} binning to get all the flux in one channel. The colour scale is -0.150 mJy (black) to 0.150 mJy (white). The green contours are 3σ , 4σ and 5σ , and the grey contour is -3σ . The cross marks the position of the ALMA source. We clearly detect $^{12}\text{CO}(2-1)$ emission associated with the ALMA source. Right: the $^{12}\text{CO}(2-1)$ spectrum of ALESS65.1 binned into 200 km s^{-1} channels and extracted at the ALMA position (black solid line). The red dashed line shows the spectrum binned into 600 km s^{-1} channels for maximum sensitivity.

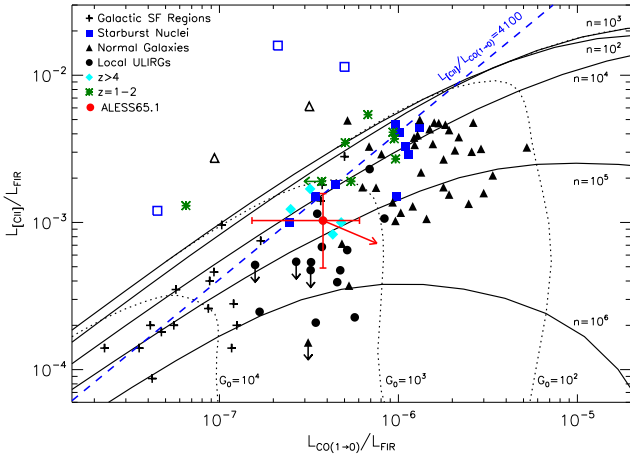


Figure 2. $L_{[\text{C II}]} / L_{\text{FIR}}$ versus $L_{\text{CO}(1-0)} / L_{\text{FIR}}$ for ALESS65.1 (red point with upper limit on $L_{\text{CO}(1-0)} / L_{\text{FIR}}$) compared with Galactic star-forming regions, starburst nuclei, normal galaxies, local ULIRGs, and high-redshift ($z > 4$) sources. Empty symbols indicate low-metallicity sources, which lie at high $L_{[\text{C II}]} / L_{\text{CO}(1-0)}$. Black lines represent the solar metallicity PDR model calculations for gas density (n) and FUV field strength (G_0) from Kaufman et al. (1999). This figure is adapted from Stacey et al. (2010) with additional data from Walter et al. (2012), Wagg et al. (2012, 2014), De Breuck et al. (2014) and Rawle et al. (2014). ALESS65.1 has a higher $L_{[\text{C II}]} / L_{\text{FIR}}$ ratio than that found in most local ULIRGs, consistent with other $z > 4$ SMGs, but its $L_{[\text{C II}]} / L_{\text{CO}}$ ratio is similar to local starbursts and other $z > 1$ sources. The red arrow indicates geometric corrections to the CO emission and non-PDR corrections to the [C II] emission, but this would apply to all galaxies in the figure and so does not affect the relative position of ALESS65.1 on the diagram compared to the other galaxies.

and at the 5.1σ level in the 600 km s^{-1} cube (see Fig. 2). From a Gaussian fit to the line, we find an integrated line flux density of $112 \pm 35 \text{ mJy km s}^{-1}$, an FWHM of $620 \pm 120 \text{ km s}^{-1}$, and a small offset from the [C II] of $140 \pm 70 \text{ km s}^{-1}$.

3 DISCUSSION

The observed and derived properties of ALESS65.1 are summarised in Table 1. The total cold gas ($\text{H}_2 + \text{He}$) mass in ALESS65.1 can be estimated from the CO(2–1) line luminosity. Following Solomon & Vanden Bout (2005), the line luminosity is $L'_{\text{CO}(2-1)} = 2.16 \pm 0.67 \times 10^{10} \text{ K km s}^{-1} \text{ pc}^2$. If we assume the gas is thermalized (i.e. intrinsic brightness temperature and line luminosities are independent of J transition), so $L'_{\text{CO}(2-1)} = L'_{\text{CO}(1-0)}$, and a CO-to- H_2 conversion factor $\alpha = 0.8 M_{\odot} (\text{K km s}^{-1} \text{ pc}^2)^{-1}$, the total cold gas mass is estimated to be $M_{\text{gas}} = 1.7 \pm 0.5 \times 10^{10} M_{\odot}$.

Table 1. Observed and derived properties of ALESS65.1.

Parameter	Value	Reference
$z_{[\text{C II}]}$	4.4445 ± 0.0005	S12
$I_{[\text{C II}]}$	$5.4 \pm 0.7 \text{ Jy km s}^{-1}$	S12
$\text{FWHM}_{[\text{C II}]}$	$470 \pm 35 \text{ km s}^{-1}$	S12
$L_{[\text{C II}]}$	$(3.2 \pm 0.4) \times 10^9 L_{\odot}$	S12
L_{FIR}	$(3.1^{+1.9}_{-1.6}) \times 10^{12} L_{\odot}$	This Letter
$I_{\text{CO}(2-1)}$	$0.112 \pm 0.035 \text{ Jy km s}^{-1}$	This Letter
$\text{FWHM}_{\text{CO}(2-1)}$	$620 \pm 120 \text{ km s}^{-1}$	This Letter
M_{gas}	$(1.7 \pm 0.5) \times 10^{10} M_{\odot}$	This Letter
$L_{\text{CO}(2-1)}$	$(8.45 \pm 2.64) \times 10^6 L_{\odot}$	This Letter
$L'_{\text{CO}(2-1)}$	$(2.16 \pm 0.67) \times 10^{10} \text{ K km s}^{-1} \text{ pc}^2$	This Letter

This is consistent with the gas mass found in other $z > 4$ SMGs (Schinnerer et al. 2008; Daddi et al. 2009a; Coppin et al. 2010; Walter et al. 2012). We caution that this gas mass is dependent on the poorly known CO-to- H_2 conversion factor α . Discs like the Milky Way have relatively high values of $\alpha \sim 3$ –5, while a smaller value, $\alpha = 0.8$, is appropriate for local ULIRGs (e.g. Downes & Solomon 1998) and is the value commonly adopted for high-redshift SMGs (but Bothwell et al. 2013 assume $\alpha = 1$).

The gas and stellar mass estimates for ALESS65.1 can be combined to derive a total baryonic mass of the galaxy. The stellar mass of the galaxy was estimated from the rest-frame absolute H -band magnitude to be $M_* \sim 9 \times 10^{10} M_{\odot}$ (S12), so the gas fraction is modest with $M_{\text{gas}} / M_* \sim 0.2$. The total baryonic mass $M_{\text{bary}} = M_{\text{gas}} + M_*$ is $\sim 10.7 \times 10^{10} M_{\odot}$. This is consistent with the dynamical mass for ALESS65.1, based on the spatial extent of the marginally resolved [C II] line, of $M_{\text{dyn}} \sin^2(i) \sim (3.4 \pm 1.8) \times 10^{10} M_{\odot}$ (S12). The baryonic and dynamical mass estimates suggest an inclination angle of about 30 deg for ALESS65.1, albeit with considerable uncertainty.

ALESS65.1 is detected at $870 \mu\text{m}$ in continuum by ALMA and marginally detected by *Herschel* (S12). Its total rest-frame IR (8–1000 μm) luminosity was estimated in S12 to be $(2.0 \pm 0.4) \times 10^{12} L_{\odot}$. A more careful deblending analysis has determined that the source is not detected in *Herschel* photometry (Swinbank et al. 2014). We estimate a revised IR luminosity for ALESS65.1 by fitting the IR spectral energy distribution (SED) using the method of Swinbank et al. (2014) but with a fixed redshift of $z = 4.44$, resulting in $\text{LIR} (8\text{--}1000 \mu\text{m}) = (3.9^{+1.8}_{-1.5}) \times 10^{12} L_{\odot}$ and $\text{LIR} (42\text{--}122 \mu\text{m}) = (3.1^{+1.9}_{-1.6}) \times 10^{12} L_{\odot}$. This is greater than the IR luminosity estimate of S12 due to the much better modelling of the detection limits of the *Herschel* SPIRE maps. This IR luminosity corresponds to an SFR of $\sim (670 \pm 310) M_{\odot} \text{ yr}^{-1}$ using the conversion of Kennicutt (1998). The gas depletion time-scale, $\tau = M_{\text{gas}} / \text{SFR} = 25 \pm 15 \text{ Myr}$, is similar to the gas depletion rates of other high-redshift SMGs (Schinnerer et al. 2008; Coppin et al. 2010). Assuming there is no further gas infall and there is 100 per cent efficiency in converting the gas to stars, the star formation is effectively shut off at $z \sim 4.4$ and this galaxy would appear red and dead by $z \sim 3$ (750 Myr after gas depletion). This short gas depletion time-scale therefore provides further evidence that $z > 4$ SMGs have the gas consumption time-scales necessary to be the progenitors of the most distant red-and-dead ‘ellipticals’, those found at $z \gtrsim 3$ (Marchesini et al. 2010; Muzzin et al. 2013).

We next examine the physical conditions of the gas in ALESS65.1 using the [C II] and $^{12}\text{CO}(2-1)$ detections. The $L_{[\text{C II}]} / L_{\text{FIR}}$ versus $L_{\text{CO}(1-0)} / L_{\text{FIR}}$ diagram is a powerful diagnostic as these two ratios are sensitive to gas density n and the incident far-ultraviolet (FUV) flux G_0 (Stacey et al. 1991). Fig. 2 shows ALESS65.1 compared with other low- and high-redshift galaxies, and solar metallicity photodissociation region (PDR) model curves (Kaufman et al. 1999). This diagram can be used to roughly estimate both n and G_0 for a galaxy, but with the following assumptions: (i) the [C II] emission comes mainly from PDRs, with little contribution from the diffuse ionized medium or cosmic-ray-heated gas, and (ii) AGN and their related X-Ray Dissociation Regions do not contribute significantly to the FIR and [C II] luminosity. To be consistent with both De Breuck et al. (2011) and Stacey et al. (2010), in Fig. 2 we assume $L_{\text{CO}(2-1)} / L_{\text{CO}(1-0)} = 7.2$, which is 90 per cent of its value if the gas was fully thermalized and optically thick. We note that this is consistent with Bothwell et al. (2013) who find $L_{\text{CO}(2-1)} / L_{\text{CO}(1-0)} = 6.72 \pm 1.04$ for $z \sim 2$ SMGs. Cosmic ray rates are greater in starbursts compared to normal galaxies but this does not seem to result in higher [C II]/CO

ratios, so cosmic ray ionization does not appear to dominate the $[\text{C II}]/\text{CO}$ ratio in local galaxies (De Breuck et al. 2011). In Huynh et al. (2013), we found that ALESS65.1 is not detected in the 250 ks *Chandra* X-Ray observations of this region (Lehmer et al. 2005), so it is not an unobscured luminous QSO ($L_{3-44 \text{ keV}} \lesssim 2-3 \times 10^{44} \text{ erg s}^{-1}$, for $N_{\text{H}} = 0-10^{23.5} \text{ cm}^{-2}$; see also Wang et al. 2013). Furthermore, a decomposition of the mid-infrared and FIR SED implied that the AGN contribution to the total FIR luminosity is $\lesssim 10$ per cent (Huynh et al. 2013). ALESS65.1 therefore appears to be dominated by star formation processes and the AGN contribution to $[\text{C II}]$ and L_{FIR} is likely to be minimal.

In examining the PDR physical conditions, we multiply the $^{12}\text{CO}(2-1)$ flux by a factor of 2 to account for detecting CO emission only from the illuminated PDR side (Kaufman et al. 1999; Hailey-Dunsheath et al. 2010), and also multiply the $[\text{C II}]$ flux by a factor of 0.7 to remove non-PDR contributions (e.g. Hailey-Dunsheath et al. 2010; Stacey et al. 2010). The ^{12}CO geometry correction applies to all galaxies in Fig. 2, and so does not affect the relative position of ALESS65.1 on the diagram compared to other galaxies. Using the Kaufman et al. (1999) models, we find ALESS65.1 has $G_0 \sim 10^{3.25}$ (where G_0 is in units of the Habing field, $1.6 \times 10^{-3} \text{ ergs cm}^{-2} \text{ s}^{-1}$) and $n \sim 10^{4.6} \text{ cm}^{-3}$ (Fig. 2). Such an FUV radiation field is higher than the FUV fields seen in low-redshift normal galaxies, but it is consistent with the strong FUV fields seen in some local starbursts and $z > 1$ galaxies. The $z > 4$ SMGs shown in Fig. 2 have inferred FUV fields at the low-end of nearby ULIRGs, the local analogues of SMGs. The estimates of G_0 and n implies a PDR temperature $\sim 300 \text{ K}$ (Kaufman et al. 1999) for ALESS65.1. Using equation 1 from Hailey-Dunsheath et al. (2010), we estimate the atomic gas associated with the PDR to be approximately $3 \times 10^9 M_{\odot}$, which is ~ 20 per cent of the total cold gas mass. This is similar to the fraction found in a similar SMG, LESS J033229.4, at $z \sim 4.76$ (De Breuck et al. 2014), redshift 1–2 star-forming galaxies (Stacey et al. 2010) and local IR bright galaxies (Stacey et al. 1991).

Local starbursts and Galactic OB star-forming regions lie on a line with $[\text{C II}]/\text{CO}$ luminosity ratios of about 4100 in Fig. 2. Higher $[\text{C II}]/\text{CO}$ ratios can be found in low-metallicity systems, such as 30 Doradus in the LMC, where the size of the $[\text{C II}]$ emitting envelope of the cloud (relative to the CO emitting core) is much larger than in more metal-rich systems (Stacey et al. 1991). Metallicity is expected to affect the $[\text{C II}]/\text{CO}$ ratios of the highest redshift galaxies because the ISMs of the youngest galaxies are expected to be less enriched by supernova. However, such enrichment appears to occur very quickly. For example, LESS J033229.4 at $z = 4.76$ has a $[\text{C II}]/\text{CO}$ ratio of ~ 5000 (De Breuck et al. 2014), suggesting near solar metallicity (see also Nagao et al. 2012). ALESS65.1 has $L_{[\text{C II}]} / L_{\text{CO}} \sim 2700$, which also indicates that the gas is not of low metallicity.

The FUV radiation fields, G_0 , of ALESS65.1 and four other $z > 4$ SMGs shown in Fig. 2, LESS J033229.4 (De Breuck et al. 2014), HDF850.1 (Walter et al. 2012), BRI 1202-0725 (Wagg et al. 2012, 2014) and HLS0918 (Rawle et al. 2014), are similar to that of local starbursts, but these distant galaxies have a much higher FIR luminosity, leading to suggestions that they are scaled-up versions of local starbursts. For a given L_{FIR} , the size of the emission region will increase for smaller G_0 . Following Stacey et al. (2010), we scale up from M82 using two laws from Wolfire, Tielens, & Hollenbach (1990) to constrain the size: $G_0 \propto \lambda L_{\text{FIR}} / D^3$ if the mean free path of a UV photon λ is small and $G_0 \propto L_{\text{FIR}} / D^2$ if the mean free path of a UV photon is large. Applying these relations and using $G_0 = 10^{3.25}$ for ALESS65.1 yields a diameter of 1.2–2.4 kpc. This is consistent with the marginally resolved $[\text{C II}]$ data which shows ALESS65.1 has a possible extent of $3.3 \pm 1.7 \text{ kpc}$ (S12). We use

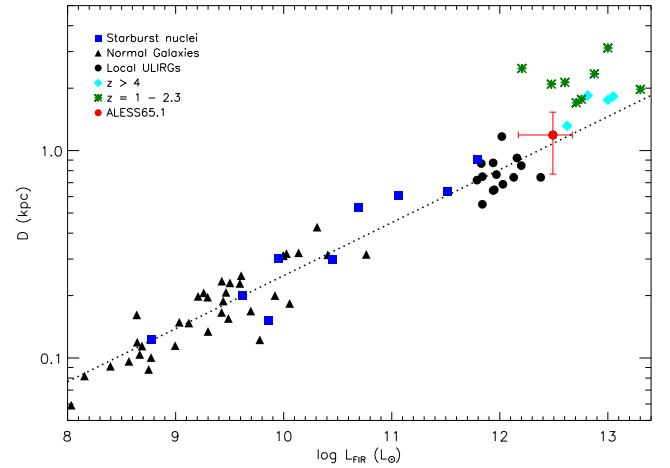


Figure 3. Size, D , versus L_{FIR} for galaxies in Fig. 2. The size is estimated using $G_0 \propto \lambda L_{\text{FIR}} / D^3$ and M82 physical parameters. G_0 is estimated from the $[\text{C II}]/L_{\text{FIR}}$ and $\text{CO}(1-0)/L_{\text{FIR}}$ ratios and Kaufman et al. (1999) PDR models (Fig. 2). Galaxies at $z > 1$ appear to lie above the local ‘trend’ (dashed line), which supports the hypothesis that they have more extended star-forming regions.

the $G_0 \propto \lambda L_{\text{FIR}} / D^3$ relation and M82 scaling parameters to estimate sizes of the star-forming regions of galaxies plotted in Fig. 2. Fig. 3 shows that the starburst in all $z > 4$ SMGs appears to be extended over galactic scales, and galaxies at $z > 1$ appear to lie above the locus delineated by local normal galaxies, local starbursts and nearby ULIRGs (Fig. 3), with moderate redshift ($1 < z < 2.3$) SMGs lying more above the local ‘trend’ than the $z > 4$ SMGs. This further suggests that starburst regions in distant galaxies are larger than in local galaxies of similar luminosity. There are caveats in interpreting Fig. 3 however: the G_0 estimate has significant uncertainties because of the large uncertainties in the line luminosity ratios used in Fig. 2; the scaling constant maybe different to that of M82 for the different galaxy samples; and the sample sizes at $z > 1$ and $z > 4$ are small and have no galaxies with $L_{\text{FIR}} < 10^{12} L_{\odot}$.

In this work, we have assumed a single-phase ISM, but ALESS65.1 may have a multiphase ISM. The spatially resolved ^{12}CO , ^{13}CO and C^{18}O study of the gravitationally-magnified SMG SMM J2135–0102 found that it has an ISM best described by a warm compact component surrounded by a cooler more extended one (Danielson et al. 2011, 2013; Swinbank et al. 2011). A multi-component ISM analysis is not currently possible due to the limitations of existing ^{12}CO data, but future higher resolution line studies with ALMA may find a similar multicomponent ISM for ALESS65.1.

4 CONCLUSION

We have observed ALESS65.1 for 40 h to search for $^{12}\text{CO}(2-1)$ emission in this $z = 4.44$ SMG. The line is detected at an $\sim 5\sigma$ level with an integrated line flux density of $112 \pm 35 \text{ mJy km s}^{-1}$ and an FWHM of $620 \pm 120 \text{ km s}^{-1}$. We find a $^{12}\text{CO}(2-1)$ line luminosity of $L_{\text{CO}(2-1)} = 8.5 \times 10^6 L_{\odot}$ and a cold gas mass of $M_{\text{gas}} \sim 1.7 \times 10^{10} M_{\odot}$. This implies a gas depletion time-scale in ALESS65.1 of 25 Myr, comparable to other $z > 4$ SMGs and consistent with this high-redshift population being the progenitors of $z \sim 3$ red-and-dead galaxies.

We examined the physical conditions of the gas in ALESS65.1 using the $L_{[\text{C II}]} / L_{\text{FIR}}$ versus $L_{\text{CO}(1-0)} / L_{\text{FIR}}$ diagram. We find

ALESS65.1 has a strong FUV field $G_0 \sim 10^{3.25}$ comparable to some local starbursts, but lower than that seen in most nearby ULIRGs, the local population with IR luminosities similar to ALESS65.1. The observed [C II] to FIR ratio, $L_{[\text{C II}]} / L_{\text{FIR}} = 1.0 \times 10^{-3}$, is high compared to local ULIRGs (as noted by S12). Combined with $L_{[\text{C II}]} / L_{\text{CO}} \sim 2700$, this high [C II] to FIR ratio is consistent with ALESS65.1 having more extended regions of intense star formation than local ULIRGs. The [C II]/CO ratio provides no evidence for low-metallicity gas in ALESS65.1.

A larger study of [C II] and ^{12}CO in distant starbursts is needed to confirm whether the majority of $z > 4$ starbursts have enhanced [C II] emission compared to their local analogues, and whether this is because of metallicity effects, the relative size of PDR regions, or other effects. Future ALMA surveys will shed further light on the physical conditions of the gas in star-forming galaxies in the early Universe.

ACKNOWLEDGEMENTS

IRS acknowledges support from the STFC (ST/I001573/1), the ERC Advanced Investigator Programme DUSTYGAL 321334 and a Royal Society Wolfson Merit Award. VS acknowledges the Group of Eight (Go8) fellowship and funding from the European Union's Seventh Frame-work program under grant agreement 337595 (ERC Starting Grant, 'CoSMass'). BE acknowledges funding through MINECO grant AYA2010-21161-CO2-01. The Australia Telescope is funded by the Commonwealth of Australia for operation as a National Facility managed by CSIRO.

REFERENCES

- Biggs A. D., Ivison R. J., 2008, MNRAS, 385, 893
 Blain A. W., Smail I., Ivison R. J., Kneib J.-P., Frayer D. T., 2002, Phys. Rep., 369, 111
 Bothwell M. S. et al., 2013, MNRAS, 429, 3047
 Capak P. et al., 2008, ApJ, 681, L53
 Capak P. L. et al., 2011, Nature, 470, 233
 Carilli C. L. et al., 2010, ApJ, 714, 1407
 Carilli C. L., Hodge J., Walter F., Riechers D., Daddi E., Dannerbauer H., Morrison G. E., 2011, ApJ, 739, L33
 Carilli C. L., Walter F., 2013, ARA&A, 51, 105
 Chapman S. C., Smail I., Windhorst R., Muxlow T., Ivison R. J., 2004, ApJ, 611, 732
 Chapman S. C., Blain A. W., Smail I., Ivison R. J., 2005, ApJ, 622, 772
 Cimatti A. et al., 2008, A&A, 482, 21
 Combes F. et al., 2012, A&A, 538, L4
 Coppin K. E. K. et al., 2009, MNRAS, 395, 1905
 Coppin K. E. K. et al., 2010, MNRAS, 407, L103
 Cox P. et al., 2011, ApJ, 740, 63
 Crawford M. K., Genzel R., Townes C. H., Watson D. M., 1985, ApJ, 291, 755
 Daddi E., Dannerbauer H., Krips M., Walter F., Dickinson M., Elbaz D., Morrison G. E., 2009a, ApJ, 695, L176
 Daddi E. et al., 2009b, ApJ, 694, 1517
 Danielson A. L. R. et al., 2011, MNRAS, 410, 1687
 Danielson A. L. R. et al., 2013, MNRAS, 436, 2793
 De Breuck C., Maiolino R., Caselli P., Coppin K., Hailey-Dunsheath S., Nagao T., 2011, A&A, 530, L8
 De Breuck C. et al., 2014, A&A, 565, A59
 Downes D., Solomon P. M., 1998, ApJ, 507, 615
 Emonts B. H. C. et al., 2011, MNRAS, 415, 655
 Emonts B. H. C. et al., 2014, MNRAS, 438, 2898
 Gooch R., 1996, in Jacoby G. H., Barnes J., eds, ASP Conf. Ser. Vol. 101, Astronomical Data Analysis Software and Systems V. Astron. Soc. Pac., San Francisco, p. 80
 Hailey-Dunsheath S., Nikola T., Stacey G. J., Oberst T. E., Parshley S. C., Benford D. J., Staguhn J. G., Tucker C. E., 2010, ApJ, 714, L162
 Heiles C., 1994, ApJ, 436, 720
 Hodge J. A., Carilli C. L., Walter F., de Blok W. J. G., Riechers D., Daddi E., Lentati L., 2012, ApJ, 760, 11
 Hodge J. A. et al., 2013, ApJ, 768, 91
 Huynh M. T. et al., 2013, MNRAS, 431, L88
 Ivison R. J., Smail I., Papadopoulos P. P., Wold I., Richard J., Swinbank A. M., Kneib J.-P., Owen F. N., 2010a, MNRAS, 404, 198
 Ivison R. J. et al., 2010b, A&A, 518, L35
 Karim A. et al., 2013, MNRAS, 432, 2
 Kaufman M. J., Wolfire M. G., Hollenbach D. J., Luhman M. L., 1999, ApJ, 527, 795
 Kennicutt R. C., Jr, 1998, ARA&A, 36, 189
 Knudsen K. K., Kneib J.-P., Richard J., Petitpas G., Egami E., 2010, ApJ, 709, 210
 Lehmer B. D. et al., 2005, ApJS, 161, 21
 Madden S. C., Geis N., Genzel R., Herrmann F., Jackson J., Poglitsch A., Stacey G. J., Townes C. H., 1993, ApJ, 407, 579
 Marchesini D. et al., 2010, ApJ, 725, 1277
 Middelberg E., Sault R. J., Kesteven M. J., 2006, PASA, 23, 147
 Muzzin A. et al., 2013, ApJ, 777, 18
 Nagao T., Maiolino R., De Breuck C., Caselli P., Hatsukade B., Saigo K., 2012, A&A, 542, L34
 Rawle T. D. et al., 2014, ApJ, 783, 59
 Riechers D. A. et al., 2010, ApJ, 720, L131
 Sault R. J., Killeen N. E. B., 1999, MIRIAD User's Guide. Australia Telescope National Facility, Sydney
 Schinnerer E. et al., 2008, ApJ, 689, L5
 Simpson J. et al., 2014, ApJ, 788, 125
 Smolčić V. et al., 2011, ApJ, 731, L27
 Smolčić V. et al., 2012, ApJS, 200, 10
 Solomon P. M., Vanden Bout P. A., 2005, ARA&A, 43, 677
 Stacey G. J., Geis N., Genzel R., Lugten J. B., Poglitsch A., Sternberg A., Townes C. H., 1991, ApJ, 373, 423
 Stacey G. J., Hailey-Dunsheath S., Ferkinhoff C., Nikola T., Parshley S. C., Benford D. J., Staguhn J. G., Fiolet N., 2010, ApJ, 724, 957
 Swinbank A. M., Chapman S. C., Smail I., Lindner C., Borys C., Blain A. W., Ivison R. J., Lewis G. F., 2006, MNRAS, 371, 465
 Swinbank A. M. et al., 2011, ApJ, 742, 11
 Swinbank A. M. et al., 2012, MNRAS, 427, 1066 (S12)
 Swinbank A. M. et al., 2014, MNRAS, 438, 1267
 Vieira J. D. et al., 2013, Nature, 495, 344
 Wagg J. et al., 2012, ApJ, 752, L30
 Wagg J. et al., 2014, ApJ, 783, 71
 Walter F. et al., 2012, Nature, 486, 233
 Wang S. X. et al., 2013, ApJ, 778, 179
 Wardlow J. L. et al., 2011, MNRAS, 415, 1479
 Weiß A. et al., 2009, ApJ, 707, 1201
 Weiß A. et al., 2013, ApJ, 767, 88
 Wolfire M. G., Tielens A. G. G. M., Hollenbach D., 1990, ApJ, 358, 116
 Yun M. S. et al., 2012, MNRAS, 420, 957

This paper has been typeset from a $\text{\TeX}/\text{\LaTeX}$ file prepared by the author.